JOC The Journal of Organic Chemistry

Article

pubs.acs.org/joc

Near-Infrared Fluorescent Thienothiadiazole Dyes with Large Stokes Shifts and High Photostability

Yanbing Zhang, Shane A. Autry, Louis E. McNamara, Suong T. Nguyen, Ngoc Le, Phillip Brogdon, Davita L. Watkins, Nathan I. Hammer, and Jared H. Delcamp*

Department of Chemistry and Biochemistry, University of Mississippi, University, Mississippi 38677, United States

Supporting Information

ABSTRACT: A series of near-infrared (NIR) organic emissive materials were synthesized and the photophysical properties analyzed. The donor−acceptor−donor materials were designed with thienopyrazine and thienothiadiazole acceptor groups with thiophene-, furan-, and triphenylamine-based donor groups. The absorption and emission spectra were found to be widely tunable on the basis of the donor and acceptor groups selected. Computational analysis confirms these materials undergo an intramolecular charge-transfer event upon photoexcitation. Large Stokes shifts of ∼150 nm were observed and rationalized by computational analysis of geometry changes in the excited state. Fluorescence studies on the dye series reveal maximum peak emission wavelengths near 900 nm and a quantum yield exceeding 16% for 4,6-bis(2-thienyl)thieno[3,4-*c*][1,2,5]thiadiazole. Additionally, several dyes were found to have reasonable quantum yields within this NIR region (>1%), with emission wavelengths reaching 1000 nm at the emission curve onset. Photostability studies were conducted on these materials in an ambient oxygen environment, revealing excellent stability in the presence of oxygen from all the dyes studied relative to a benchmark cyanine dye (ICG) during photoexcitation with exceptional photostability from the 4,6-bis(5′-dodecyl-[2,2′-bithiophene]-5-yl)thieno[3,4-*c*][1,2,5]thiadiazole derivative.

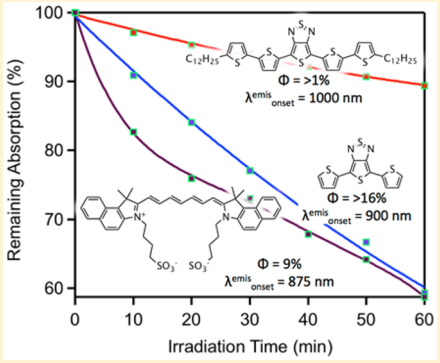

INTRODUCTION

A wide array of applications exist for emissive materials, with research interest recently increasing regarding materials in the near-infrared (NIR) region. Among potential applications for these materials, optical biological imaging is becoming a prosperous field due to the high sensitivity and resolution without invasive measures.[1] This technique can use small organic molecules to absorb and emit photons in the therapeutic window of 650−1400 nm (depending on the tissue present), where the absorption and autofluorescence of the biological matrix are the lowest, leading to the deepest penetration depth.[2−4] Higher resolution in this region is desirable and is directly related to increased Stokes shifts (change in energy between absorption and emission curves), high fluorescence quantum yields (ratio of the number of photons emitted to the number of photons absorbed), and absorption as well as emission within the therapeutic window. Materials with these properties could offer new advances in emissive material applications such as biological imaging.[5−23] One of the most intriguing dyes for imaging applications is based on a donor−acceptor−donor (D−A−D) design with a benzobisthiadiazole acceptor and two triphenylamine donor groups (CH1055-PEG) which emits in the NIR II window (Figure 1); however, the fluorescence quantum yield can still be improved (ϕ = 0.3%).[24] Further understanding of the fundamental photophysical properties of NIR conjugated systems is needed to rationally design future generations of applied materials with tailored emissive properties for numerous applications, including biological imaging.

Recently, our groups evaluated a thienopyrazine (TPz)-based D−A−D dye series,[25] which has large Stokes shifts when compared to many common NIR dyes, such as those based on cyanine (ICG), of up to 200 nm with a 4% quantum yield (Figure 1). Due to steric interactions between the thienopyrazine ring and triarylamine rings, significant reorganization energy is needed upon photoexcitation to reach the lowest energy excited-state geometry. This high reorganization energy results in a large Stokes shift. Despite these impressive metrics, these dyes can be improved by a shifting of the absorption and emission profiles further into the NIR region as is needed for many applications.[1,4] Herein, we report a fundamental study in tuning the photophysical properties of D−A−D dyes by designing a new series of NIR dyes aimed at maintaining the desired properties of the prior TPz series while accessing lower energy photons.

The low-energy absorption band of the TPz-based dyes results from the transfer of electron density from the donor (D) regions to the acceptor (A) region within the D−A−D framework. We reasoned this band could be shifted toward longer wavelengths by (1) using a stronger accepting motif, (2) reducing the acceptor−donor dihedral angle, and (3) increasing the conjugation length with weaker donors in place of stronger

Received: February 21, 2017
Published: May 5, 2017

DOI: 10.1021/acs.joc.7b00422
J. Org. Chem. 2017, 82, 5597−5606

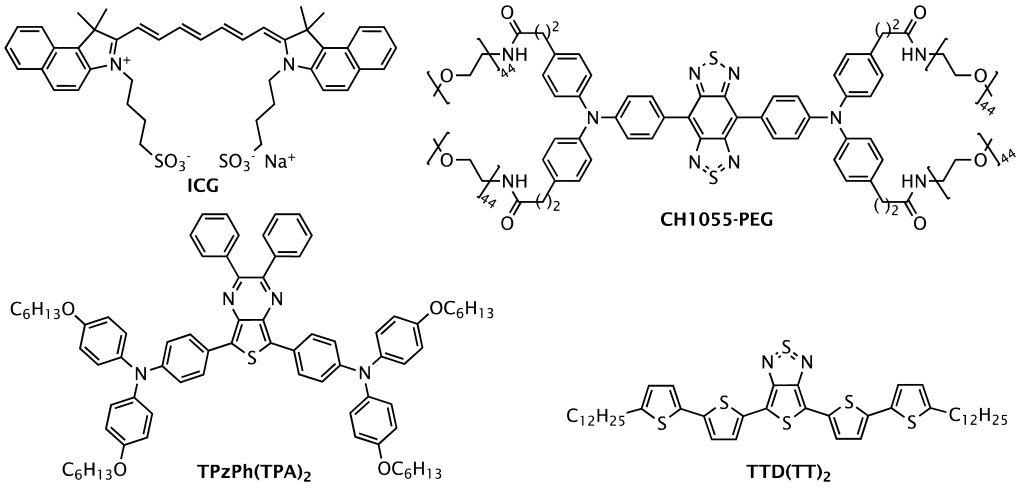

Figure 1. Known ICG,[7] CH1055-PEG,[24] and TPzPh(TPA)$_2$[25] NIR emissive material structures compared to target dye TTD(TT)$_2$.

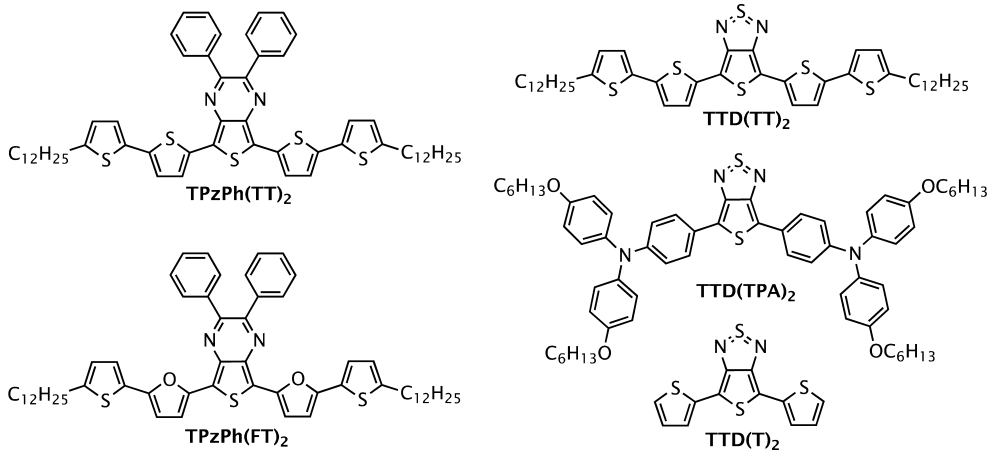

Figure 2. Target NIR emissive compounds TPzPh(TT)$_2$, TPzPh(FT)$_2$, TTD(TT)$_2$, TTD(TPA)$_2$, and TTD(T)$_2$.

Scheme 1. Synthetic Route to TPzPh(TT)$_2$, TPzPh(FT)$_2$, TTD(TT)$_2$, and TTD(TPA)$_2$[a]

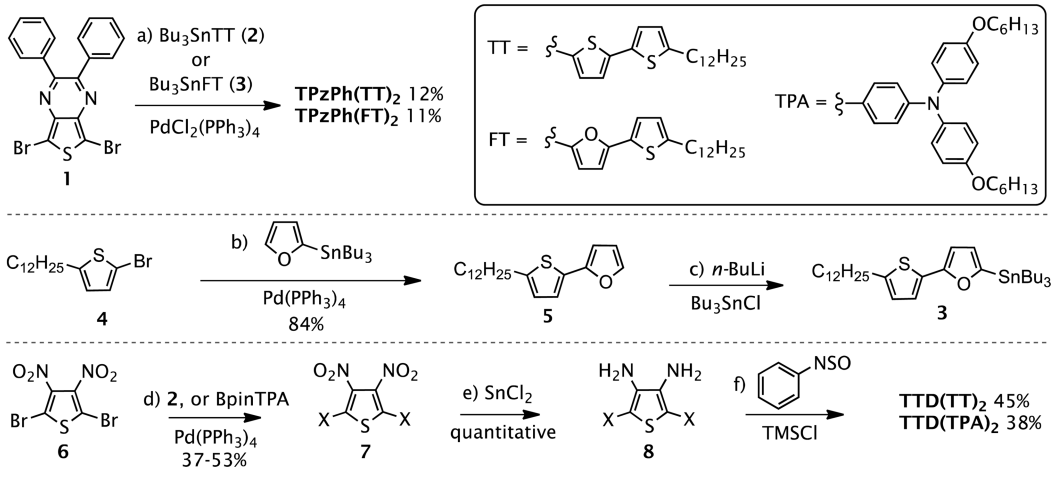

[a]Reagents and conditions: (a) 10% PdCl$_2$(PPh$_3$)$_2$, 50 °C, overnight, 11−12%; (b) 10% Pd(PPh$_3$)$_4$, toluene/DMF, reflux, overnight, 84%; (c) *n*-BuLi (1.5 equiv), Bu$_3$SnCl (0.4 equiv), 0.1 M THF, −78 °C, overnight, quantitative; (d) 10% Pd(PPh$_3$)$_4$, toluene or dioxane, 24 h, 37%−53%; (e) SnCl$_2$ (10 equiv), 1.4 M conc. HCl, 1.0 M EtOH, 0.01 M DCM, room temperature, 3 days, 100%; (f) thionylaniline (2.0 equiv), (TMS)Cl (7.0 equiv), 0.2 M pyridine, room temperature, overnight, 38−68%.

donors with shorter conjugation lengths. The thienothiadiazole (TTD) building block was evaluated as a stronger acceptor with reduced steric repulsion between the donor and acceptor as a result of introducing a 5,5-fused ring system in place of the 5,6-fused TPz (Figure 2). We reasoned the release of ring strain energy from the thiadiazole ring by significantly elongating

DOI: 10.1021/acs.joc.7b00422
J. Org. Chem. 2017, 82, 5597−5606

bonds in this ring would maintain significant Stokes shifts. Additionally, we sought to evaluate the effects of replacing the previously studied triphenylamine donor with furan and thiophene linkages to both the TPz and TTD acceptors. The triphenylamine donor is a strong electron-donating group with increased steric interactions at the D−A bond, while the furan and thiophene groups are weaker electron donors with reduced sterics. While increasing the strength of donor and acceptor groups commonly leads to lower energy absorptions in small molecules, we reasoned that reduced sterics, elimination of highly resonance stabilized benzene rings, and increased conjugation length could result in lower energy absorptions from weaker donor building blocks.

To analyze our hypotheses, we selected a series of systematically targeted dyes for comparing the effects of varying donor groups on an identical thienopyrazine core. Dithiophene and furan−thiophene-based donors (TPzPh(TT)$_2$ and TPzPh(FT)$_2$) were chosen to increase the planarity as well as conjugation length to allow for lower energy photon absorption when compared to the previously reported TPzPh(TPA)$_2$. However, the Stokes shift is predicted to be significantly reduced with higher planarity dyes.[25] As the Stokes shift represents the reorganization of the dye in the excited state, varying the acceptor core to a building block with strain that can be released in the excited state can still provide a large Stokes shift without reducing the dye planarity as is needed to reach longer wavelengths. To provide a desirable reorganization energy and further shift the absorption and emission spectra into the optical therapeutic window, TTD was substituted in place of the TPzPh acceptor since thienothiadiazole is more electron deficient than thienopyrazine due in part to the inclusion of a hypervalent sulfur atom.[26] For a direct comparison of these functionalities, TTD(TT)$_2$ and TTD(TPA)$_2$ are valuable target dyes. To assess the importance of the second thiophene with TTD(TT)$_2$, TTD(T)$_2$ is targeted to analyze the resulting photophysical properties.

SYNTHESIS

All of the target NIR dyes are readily accessible through traditional transition-metal cross-coupling synthetic routes. Synthetic routes to the five target dyes can be be carried out in five or fewer linear steps from commercially available materials (Scheme 1). Several synthetic analogues of the TPzPh[27−30] and TTD[30−35] target dyes are known primarily in the polymer literature as monomer precursors for alternative applications. The synthesis of the TPzPh-based dyes began with known 5,7-dibromo-2,3-diphenylthieno[3,4-*b*]pyrazine (**1**), which undergoes Stille coupling with stannyl-TT (**2**) or stannyl-FT (**3**) (Scheme 1).[25,36,37] **3** is available in two steps beginning from bromothiophene derivative **4** and 2-(tributylstannyl)furan and then lithiation with butyllithium and quenching with tributyltin chloride to give **3**. Due to purification challenges associated with chromatographically separating the desired product from the homocoupled stannyl reagent, recrystallization was used as the final purification technique to give an 11−12% yield of the final pure desired dyes TPzPh(TT)$_2$ and TPzPh(FT)$_2$. The furan-based dye demonstrates limited stability and needs to be kept under nitrogen in the dark to reduce decomposition. The synthetic route for TTD(T)$_2$ is known and was easily repeated.[34] The remaining TTD-based dyes followed a similar route beginning from known 2,5-dibromo-3,4-dinitrothiophene (**6**), which underwent Stille coupling with Bu_3SnTT to generate **7** (X = TT). Analogously, the triphenylamine donors were installed via Suzuki coupling of **6** with TPA-pinacol boronic ester to give **7** (X = TPA). The dinitro interemediates **7** underwent quantitative reduction with $SnCl_2$ to give the diamine intermediates **8**, which were converted to the desired final dyes with thionylaniline and (TMS)Cl. Attempts to synthesize the TTD(FT)$_2$ analogue of TTD(TT)$_2$ were not successful as the diamine intermediate **8** (X = FT) had significantly lower stability and could not be successfully isolated.

RESULTS AND DISCUSSION

With the target dyes synthesized, the optical properties of the D−A−D NIR dyes were measured to reveal the effect of the different donors and acceptors on the molar absorptivity and optical band gap. The λ_{max} range for the dye series varies from 629 to 717 nm due to what appears to be a single, broad intramolecular charge-transfer band (Figure 3, Table 1).

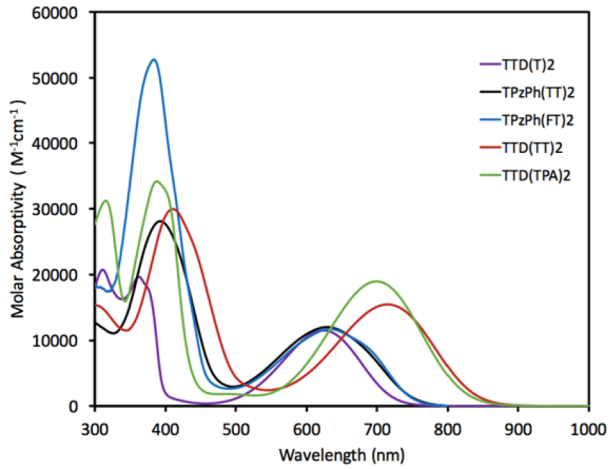

Figure 3. Absorption curves of TTD(T)$_2$, TPzPh(TT)$_2$, TPzPh(FT)$_2$, TTD(TT)$_2$, and TTD(TPA)$_2$ in toluene.

Comparison of the donor group on the dye optical properties is possible through a comparison of the previously characterized TPzPh(TPA)$_2$ and the newly reported dyes TPzPh(TT)$_2$ and TPzPh(FT)$_2$.

Interestingly, despite the lower electron-donating strength of thiophene and furan when compared with triphenylamines, the newly synthesized dyes with thiophene and furan donors are red-shifted by 29 and 33 nm, respectively, when compared with the parent dye TPzPh(TPA)$_2$. Reduced steric repulsion between the acceptor and a five-membered thiophene or furan ring when compared to the same interaction between the acceptor and a six-membered benzene promotes dye planarity enough to desirably red shift the absorption maximum. Additionally, the conjugation length is increased through the use of two aromatic heterocycles per donor in place of the single benzene in triphenylamine, further causing a bathochromic shift. The molar absorptivity is only modestly affected by the change in donor group, with TPzPh(TPA)$_2$ having a molar absorptivity of 14000 M^{-1} cm^{-1} while the TT- and FT-substituted analogues have molar absorptivities of 12000 $M^{-1}cm^{-1}$. Little difference is observed in the absorption spectra for TPzPh(TT)$_2$ and TPzPh(FT)$_2$ in the low-energy region (450−750 nm); however, in the higher energy region (350−450 nm) a significantly stronger absorption is observed for the furan derivative. TTD(TPA)$_2$ and TTD(TT)$_2$ offer a

DOI: 10.1021/acs.joc.7b00422
J. Org. Chem. 2017, 82, 5597−5606

Table 1. Photophysical Properties Measured in Toluene

dye	λ_{abs}^{max} (nm)	λ_{abs}^{onset} (nm)	ε (M^{-1} cm^{-1})	λ_{emis}^{max} (nm)	Stokes shift (nm, eV)	ϕ (%)	τ (ns)
$TPzPh(TPA)_2$[a]	600	730	14000	748	148, 0.41	4.3	1.2
$TPzPh(TT)_2$	629	770	12000	765	136, 0.35	1.2	0.9
$TPzPh(FT)_2$	633	765	12000	764	131, 0.34	4.1	0.6
$TTD(TPA)_2$	698	830	19000	875	177, 0.36	1.1	1.1
$TTD(TT)_2$	717	850	15000	877	160, 0.32	1.0	0.8
$TTD(T)_2$	624	740	12000	765	141, 0.37	16.8	2.1
ICG[b]	816	870	141000	819	3, <0.01	9.0	0.7

[a]Previously reported.[25] [b]Measured in toluene/methanol (2:1). Note: When comparing Stokes shifts of dyes, the energy comparison we focus on is in terms of electronvolts, whereas small perturbations to dye structures often lead to larger shifts in nanometer values in the NIR region compared to the higher energy regions. However, these large changes in energy in terms of nanometer numerical values in the NIR region are represented by relatively small energy changes in terms of electronvolts.

direct comparison of the thienothiadiazole with the thienopyrazine group of $TPzPh(TPA)_2$ and $TPzPh(TT)_2$. A near 100 nm red shift of the λ_{max} and λ_{onset} values in toluene is observed for the thienothiadiazole derivatives. Additionally, an increase in molar absorptivity is observed for each thienothiadiazole derivative (from 14000 to 19000 M^{-1} cm^{-1} for the TPA derivatives and from 12000 to 15000 M^{-1} cm^{-1} for the TT derivatives). Otherwise, the charge-transfer low-energy absorption peaks have similar shapes and widths for the two derivatives. The enhanced molar absorptivity and absorption of lower energy photons when using the thienothiadiazole bridge are indicative of a more planarized π-conjugated system and an enhanced electron-withdrawing strength. Removal of a thiophene from the $TTD(TT)_2$ structure to give $TTD(T)_2$ resulted in a 110 nm blue shift of the absorption spectrum onset, which clearly highlights the importance of the added electron density of the second thiophene group in the development of dyes to access low-energy photons in the NIR region.

Computational Results. To better understand the optical properties of these dyes, density functional theory (DFT) and time-dependent density functional theory (TD-DFT) computational studies were undertaken to analyze the orbital arrangement, planarity, and intramolecular charge-transfer (ICT) characteristics of the dyes. The geometry of the dyes is first optimized with the B3LYP functional and 6-311G(d,p) basis set (Figure 4, Table 2). The highest occupied molecular orbital (HOMO) and lowest unoccupied molecular orbital (LUMO) orientations are shown in Figure 4. The HOMO is delocalized across the dye from each donor and includes the thiophene region of the acceptor groups. Specifically, in the case of the TPA-based dyes, the HOMO is only substantially present on the benzene ring in conjugation with the acceptor while the two remaining TPA rings out of conjugation do not have a substantial HOMO contribution. This is in contrast to the TT- and FT-based donors where the HOMO is delocalized across the entire dye, with contributions from both rings of each donor. This observation suggests that conjugation length changes may significantly affect the lowest absorption wavelengths of these dyes. The LUMO is heavily localized on the whole acceptor building block, and substantial orbital overlap is observed on the thiophene of each acceptor. For the thienopyrazine-based dyes, the LUMO does show some orbital density on the donor region while the thienothiadiazole shows LUMO orbital density only on the acceptor region at the same isovalues. This comparison highlights the stronger electron-accepting ability of the TTD donor and results in a lower energy ICT absorption for these dyes with analogous donor

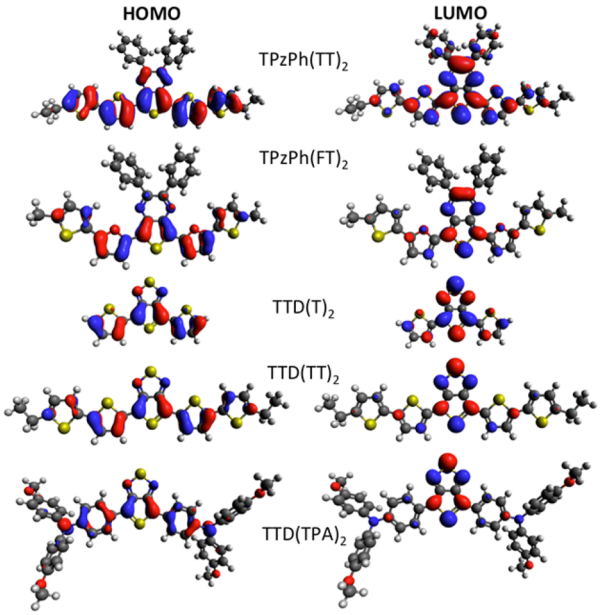

Figure 4. HOMO (left) and LUMO (right) orbitals of $TPzPh(TT)_2$, $TPzPh(FT)_2$, $TTD(T)_2$, $TTD(TT)_2$, and $TTD(TPA)_2$. Isovalues were set to 0.04.

Table 2. Computational Results from DFT and TD-DFT Analysis

dye	D−A dihedral angle	vertical transition (nm, eV)	oscillator strength
$TPzPh(TPA)_2$[a]	20	706, 1.76	0.41
$TPzPh(TT)_2$	3.7	725, 1.71	0.56
$TPzPh(FT)_2$	7.7	699, 1.77	0.49
$TTD(TPA)_2$	4.6	891, 1.39	0.50
$TTD(TT)_2$	1.0	887, 1.40	0.54
$TTD(T)_2$	0.0	725, 1.71	0.21

[a]Previously reported.[25]

groups. As previously noted, a reduction in sterics is expected when TPA is changed to a TT or FT donor group. For the TPz-acceptor-based dyes, this change in sterics from the donor is apparent as the TPA−TPz dihedral angle is 20° and the dihedral angles at the TT−TPz and TF−TPz bonds are 3.7−7.7° after geometry optimization. Changing the acceptor building block also leads to a significant reduction in sterics at the D−A bond, giving a TPA−TTD dihedral angle of 0.0° after geometry optimization. These results support the conclusion that reduced steric interactions play an important

DOI: 10.1021/acs.joc.7b00422
J. Org. Chem. 2017, 82, 5597−5606

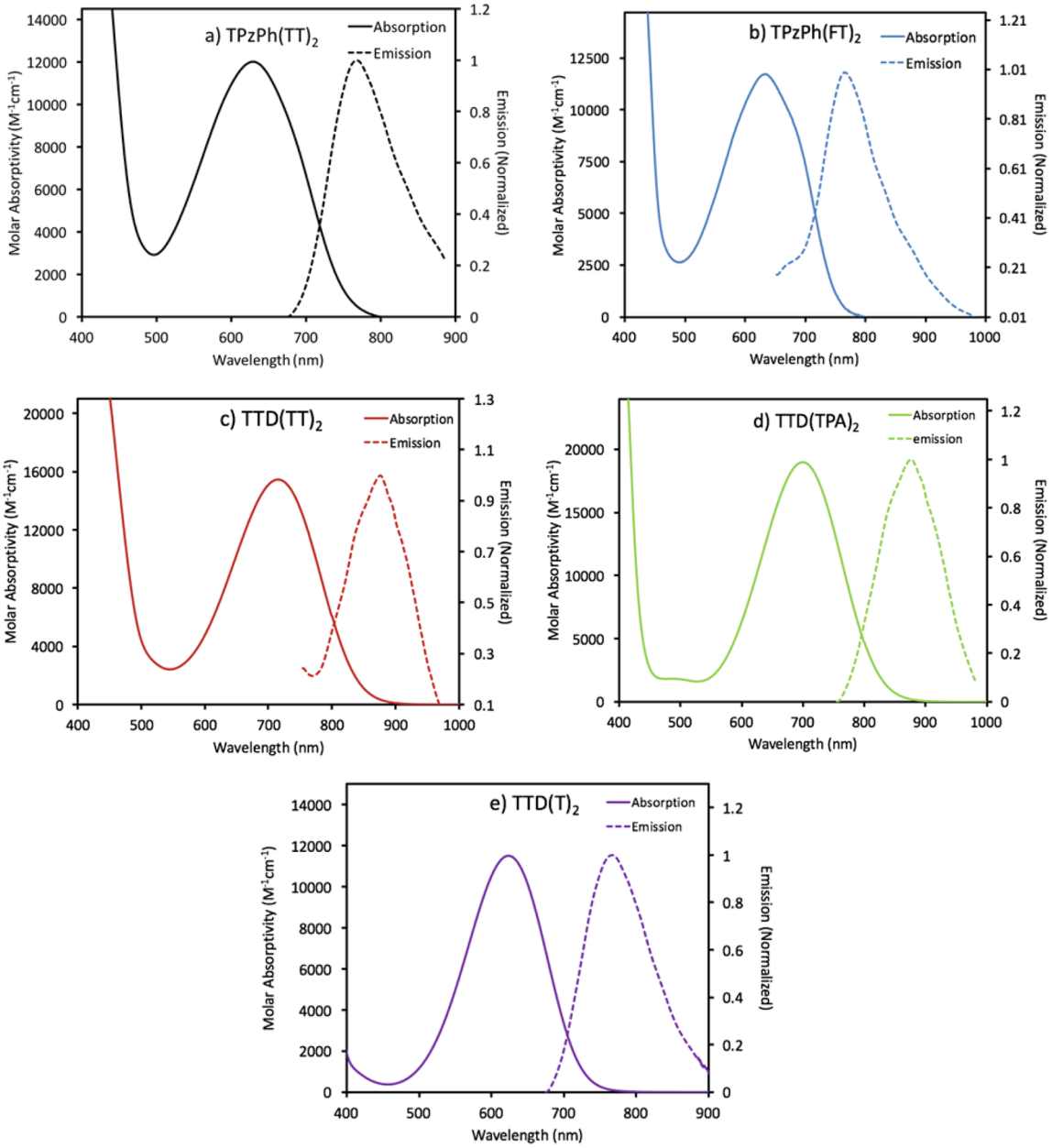

Figure 5. Absorption and emission curves of (a) $TPzPh(TT)_2$, (b) $TPzPh(FT)_2$, (c) $TTD(TT)_2$, (d) $TTD(TPA)_2$, and (e) $TTD(T)_2$ in toluene.

role in shifting the UV−vis−NIR absorption values for these dyes as changing the donor from TPA to TT or FT dramatically lowers the dihedral angle value while simultaneously causing absorption of lower energy wavelengths.

TD-DFT analysis with the B3LYP functional and 6-311G(d,p) basis set was used to analyze the predicted 10 lowest energy vertical transitions of the dyes in isolation from the optimized ground-state geometry to identify the orbitals contributing to the absorption bands observed (Table 2). The lowest energy vertical transition trends match the experimental λ_{max} trends on the basis of acceptor building block choice. However, for the donor groups TD-DFT predicts similar values for vertical transition energies. Given how close in energy the experimental absorption spectrum maxima are for the TPzPh dyes and the similar absorption spectra of the $TTD(TPA)_2$ and $TTD(TT)_2$ dyes, predicting the changes in energy with TD-DFT is challenging as only a ≤0.06 eV difference separates each dye set. The oscillator strength values are close for each of the dyes, which indicates the molar absorptivity values should be relatively close in value for each of the dyes as is observed from solution measurements. In all cases, the TD-DFT results show the lowest energy vertical transitions are dominated by HOMO−LUMO transition (>99%), with the nearest significant vertical transition substantially higher in energy by >250 nm. These results suggest the absorption bands of these dyes extending into the NIR region predominantly result from a strong ICT from a donor to acceptor region.

Emissive Properties. Having established the strong absorption of these dyes into the NIR spectral region, the emissive properties of the dyes were evaluated in toluene solutions (Figure 5, Table 1). All dyes were found to emit within the desired wavelength range, with λ_{emis} maxima ranging from 748 to 877 nm and emission curve onset values from 900 to 1000 nm. An additional requirement for biological imaging purposes is a large Stokes shift to reduce overlap of the excitation energy and emission energy as scattered excitation

DOI: 10.1021/acs.joc.7b00422
J. Org. Chem. 2017, 82, 5597−5606

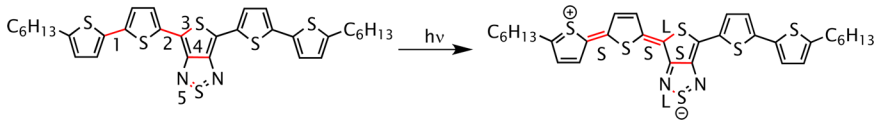

Figure 6. $TTD(TT)_2$ ground-state and excited-state bond length changes.

photons from the laser source dramatically reduce the image resolution in the absence of significant energy separation. Large Stokes shifts of 131−177 nm (0.32−0.41 eV) in toluene were observed for the dye series. Prior studies have shown the Stokes shift of $TPzPh(TPA)_2$ to originate from a substantial shift in ground-state and excited-state geometries with a dramatic change at the donor group−acceptor group dihedral angle. The Stokes shift is hypothesized to be reduced as a result of lowering steric interactions at the donor−acceptor (D−A) group bond. For the largest acceptor group, TPzPh, the following trend of Stokes shifts was observed: $TPzPh(TPA)_2$ > $TPzPh(TT)_2$ > $TPzPh(FT)_2$. This observed trend is in agreement with the predicted steric influence. The smaller acceptor group, TTD, should have a similar trend among the donor group substituents, only with a lesser extent of Stokes shift changes. This prediction was observed as the Stokes shift of $TTD(TPA)_2$ was greater than that of $TTD(FT)_2$, but lower than that of $TPzPh(TPA)_2$. Interestingly, $TTD(T)_2$ was found to have one of the largest Stokes shifts in the series in terms of electronvolt units at 0.37 eV using the smallest accepting group, and a 0.05 eV larger Stokes shift than is observed for the $TTD(TT)_2$ derivative. This implies that $TTD(T)_2$ has a greater reorganization energy than the $TTD(TT)_2$ derivative. Solvatochromic effects were evaluated via absorption and emission spectroscopy with $TTD(T)_2$ to examine the effects of the solvent polarity on the ground state and excited state (Figure S1, Supporting Information). The absorption maxima varied by 0.05 eV (14 nm) over 12 solvents with widely varied polarities. This negligible change of the absorption spectrum suggests the conformation of the molecule in the ground state is relatively unaffected by the solvent polarity. Interestingly, the emission maximum energy varied to a great extent by 0.14 eV (73 nm) over the same 12 solvents. This change is more significant and suggests a substantial reorganization of the $TTD(T)_2$ dye in the excited state. For the most polar solvent $TTD(T)_2$, which was appreciably soluble in DMSO, the largest Stokes shift was observed at 0.52 eV (220 nm). To better understand the origin of the Stokes shift for these dyes, computational chemistry was used to analyze the excited-state geometry changes. Interestingly, unlike other biological imaging dyes having a large Stokes shift resulting from dihedral angle changes between donor and acceptor rings, $TPzPh(TT)_2$, $TPzPh(FT)_2$, $TTD(TT)_2$, $TTD(FT)_2$, and $TTD(T)_2$ have substantial Stokes shifts, but no substantial change in dihedral angle has been observed as this value is already near 0° for these dyes. To probe this expectation, computational studies were carried out to optimize the first excited-state geometry.

$TTD(TT)_2$ was closely analyzed as an example dye to evaluate the origin of the observed Stokes shifts on the basis of geometry changes in the ground state (S_0) and lowest excited state (S_1; Figure 6, Table 3). In a straightforward manner, valence bond theory suggests that bonds 1 and 2 will be shortened upon excitation to the excited state as double bond character is increased upon ICT. Conversely, bond 5 should be elongated due to an increase in single bond character upon intramolecular charge transfer. Upon careful examination of the

Table 3. Comparison of C−C Bond Lengths in the Ground State (S_0) and Excited State (S_1) and the Length Changes (ΔR)

bond	S_0 bond length (Å)	S_1 bond length (Å)	ΔR (Å)
1	1.442	1.432	−0.01
2	1.425	1.402	−0.02
3	1.748	1.770	+0.02
4	1.455	1.427	−0.03
5	1.638	1.694	+0.06

calculated excited-state geometry, bond length changes in the dyes were found to be the primary reorganization event, with the largest effects seen at the TTD building block (Table 3). The lengths of bond 1 and bond 2 decrease by 0.01 and 0.02 Å, respectively, while the length of bond 5 shows the largest change by increasing 0.06 Å as predicted by valence bond theory. Interestingly, bonds 3 (0.02 Å lengthening) and 4 (0.03 Å shortening) both change significantly according to computational analysis for the ground and excited states. We rationalize the change in bond 3 length as occurring due to the loss of local aromaticity (and thus less homogeneous bond lengths) at the center thiophene ring upon ICT. Bond 4 in the ground state is significantly longer than that of the remaining thiophenes in the $TTD(TT)_2$ dye (1.46 Å versus 1.41 Å, respectively). We attribute this to the hypervalent sulfur (assuming a geometry preference similar to that of SO_2 with an AX_2N geometry) and both sp^2-hybridized nitrogens attached to the sulfur atom all preferring bond angles of 120°, which would significantly elongate bond 4 in the ground state. In the excited state some of this ring strain is released, presumably due to a partial rehybridization of the hypervalent sulfur to more of an AX_2N_2 geometry (~110° for noncyclic systems), which better matches the ring strain free five-membered ring geometry at ~110°.

In addition to inducing large Stokes shifts for better imaging resolution, high fluorescence quantum yields are important for either allowing lower dye quantities to be administered for imaging applications or enhancing the resolution at larger tissue depths with equal dye amounts administered when compared with lower fluorescence quantum yields.[25] For this series, despite large Stokes shifts, the target dyes maintain a >1% quantum yield, which improves the current state of the art emissive dye quantum yields of materials with similar Stokes shifts near this spectral region (e.g., for CH1055-PEG, ϕ = 0.3%). $TTD(TT)_2$ and $TTD(TPA)_2$ both have emission spectra reaching >950 nm. In this range, a quantum yield greater than 1% (as both of these dyes show) is notable. $TPzPh(TT)_2$, $TTD(TT)_2$, and $TTD(TPA)_2$ all demonstrated roughly similar fluorescence quantum yields of ~1% despite significantly different emission ranges, with $\lambda_{emis\ max}$ varying by 112 nm (0.21 eV). The energy gap law generally dictates that the nonradiative excited-state decay rate increases exponentially as the emission energy decreases, leading to dramatically lower quantum yields as ($\phi = k_r/(k_r + k_{nr})$), where k_r is the radiative decay rate and k_{nr} is the sum of all nonradiative decay rates.[21,38−44] This suggests the energy gap law is not the

DOI: 10.1021/acs.joc.7b00422
J. Org. Chem. 2017, 82, 5597−5606

primary factor controlling the relative quantum yields of these materials since as k_{nr} increases exponentially, an inverse effect is expected to be observed on ϕ.[21,38] To indirectly evaluate the change in k_{nr} of these dyes, fluorescence lifetimes of these materials were measured through time-correlated single-photon-counting (TCSPC) experiments where $\tau = 1/(k_r + k_{nr})$ and τ is found through the fluorescence decay curve fit (Figure 7).

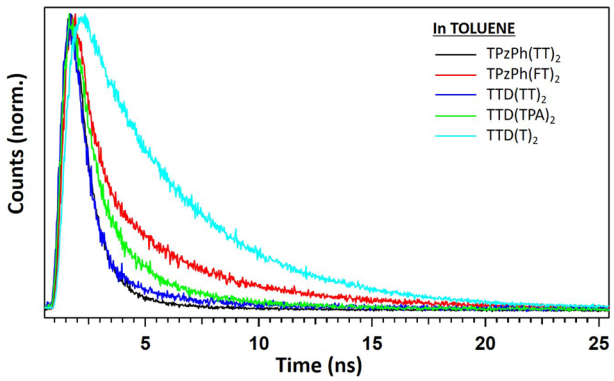

Figure 7. TCSPC fluorescent decay curves for $TPzPh(TT)_2$, $TPzPh(FT)_2$, $TTD(TPA)_2$, $TTD(TT)_2$, and $TTD(T)_2$.

Fluorescence lifetimes for the dyes are all close with a range from 2.1 to 0.6 ns. Since the measured ϕ and τ values are similar for each of the dyes, this suggests the summed rate of nonradiative decay events remains nearly constant for these dyes as the emission energies shift to lower energy values. Substantially, higher fluorescence quantum yields were observed for $TTD(T)_2$ (16.8%) and $TPzPh(FT)_2$ (4.1%). Both materials have emission maxima at similar energies (1 nm difference in energy), which eliminates energy gap law concerns for explaining the drastic difference in ϕ. Comparison of fluorescence lifetimes shows a 3.5-fold increase in τ value for $TTD(T)_2$ when compared with $TPzPh(FT)_2$. Given the 4.1-fold increase in quantum yield for $TTD(T)_2$, and the equation $k_r = \phi/\tau$ derived from the above equations, essentially no substantial change has occurred in the k_r term for either of the dyes. This suggests the dramatically improved fluorescence quantum yield of $TTD(T)_2$ comes from reducing the nonradiative decay rate by roughly 4 times that of $TPzPh(FT)_2$. This decrease in k_{nr} is potentially due to fewer thermal deactivation pathways in the more concise $TTD(T)_2$ structure. It should be noted that the ϕ of $TTD(T)_2$ is exceptionally high for a material emitting photons at >750 nm.

Photostability. A common challenge with many NIR emissive materials is low photostability of dyes during prolonged irradiation in the presence of oxygen.[45] To evaluate the photostability of these dyes, they were dissolved in toluene at a concentration of 1×10^{-5} M to maintain consistency with absorption and fluorescent quantum yield studies. The samples were then irradiated with a 150 W Xe lamp (AM 1.5 filter) at a distance of 25 cm (94.8 mW/cm^2) with a cutoff filter to remove photons higher in energy than 400 nm (Figure 8).[46] No precautions were taken for the removal of oxygen from the dye solution to evaluate the stability of the dyes under ambient conditions. The dye solutions were placed in front of the lamp for the indicated time, and then absorption spectra were taken to evaluate the percent change in λ_{max} as a result of irradiation.

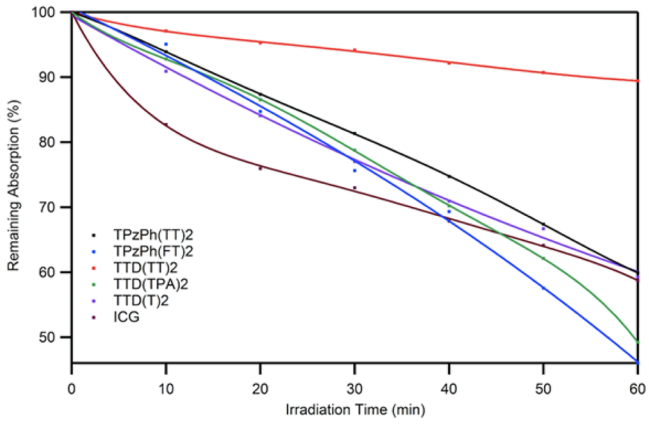

Figure 8. Photostability behavior of $TPzPh(TT)_2$, $TPzPh(FT)_2$, $TTD(TT)_2$, $TTD(TPA)_2$, and $TTD(T)_2$ in toluene and ICG in toluene/methanol (2:1).

The data are plotted in Figure 8 as the percentage of the λ_{max} absorbance remaining after irradiation.

All dyes show reasonable stability over the course of a continuous hour of irradiation and maintain ~50% to >90% of the original dye concentration. The dye stability in order from most stable to least is $TTD(TT)_2$ > $TPzPh(TT)_2$ = $TTD(T)_2$ > $TTD(TPA)_2$ > $TPzPh(FT)_2$ after 1 h of irradiation. Interestingly, among the TTD series, the thiophene-donor-based dyes were significantly more stable than the TPA-based dye. By a considerable amount, the $TTD(TT)_2$ dye was the most stable and maintained >90% dye concentration after being irradiated continuously for 1 h. When comparing the TPzPh and TTD acceptors with the TT donor group, a significantly higher stability is observed for the TTD acceptor, which suggests the decomposition pathways for the TPzPh acceptor are more facile than those for the TTD acceptor. When comparing the highest stability of the TT donor and the FT donor, a greater stability for the TT donor is clearly observed as was noted qualitatively during the synthesis of these materials. This correlates to what would be predicted on the basis of the lower resonance stabilization energy of furan when compared with thiophene (16 kcal/mol vs 29 kcal/mol), which likely plays a role in the rate of decomposition. The high photostability of $TTD(TT)_2$ is in stark contrast to the photostability of the cyanine dye ICG.[47] The key structural elements for introducing high photostability were (1) the addition of a strong electron-withdrawing group and (2) the use of planarizing, weaker donating functionality.

CONCLUSION

These results suggest the D−A−D design for NIR dyes can be used as a low-energy-absorbing and -emitting dye design with good photostability and high fluorescence quantum yields. All target dyes studied were synthesized in five reproducible steps. UV−vis−NIR spectrometry, computational studies, photostability, and emissive studies were undertaken to analyze the photophysical property changes of these dye designs. The series of five dyes synthesized in this study all absorb and emit within the NIR region with Stokes shifts from 136 to 177 nm (λ^{abs}_{onset} = 730−850 nm, λ^{emis}_{onset} = 950−1000 nm). Encouragingly, the fluorescence quantum yields of all the dyes were observed at >1% (reaching 16.8%), which is particularly intriguing as the energy gap law suggests greatly diminished fluorescence quantum yield in this spectral region. Photostability experi-

DOI: 10.1021/acs.joc.7b00422
J. Org. Chem. 2017, 82, 5597−5606

ments indicated all the dyes exhibit reasonable stabilities in the presence of ambient oxygen during continuous irradiation with TTD(TT)$_2$ showing exceptional photostability. These characteristics suggest the π-conjugated dye systems are promising candidates for future NIR emissive material applications, including biological system fluorescence imaging studies with several functional positions for tuning dyes to specific application needs.

EXPERIMENTAL SECTION

Materials. All commercially obtained reagents and solvents were used as received without further purification. 4,6-Bis(2-thienyl)thieno-[3,4-*c*][1,2,5]thiadiazole,[31] 4,6-bis(5-bromo-2-thienyl)thieno[3,4-*c*]-[1,2,5]thiadiazole,[34] 5,7-dibromo-2,3-diphenylthieno[3,4-*b*]pyrazine,[25] 2,5-dibromo-3,4-dinitrothiophene,[25] tributyl(5′-dodecyl-[2,2′-bithiophene]-5-yl)stannane,[48] and 2-bromo-5-dodecylthiophene[48] were prepared according to the literature. Thin-layer chromatography (TLC) was conducted with silica gel XHL TLC plates from Sorbent Technologies and visualized with UV and potassium permanganate staining. Flash column chromatography was performed using Sorbent Tech P60, 40−63 μm (230−400 mesh) silica gel. ^{1}H NMR spectra were recorded on Bruker Avance-300 (300 MHz) and Bruker Avance DRX-500 (500 MHz) spectrometers and are reported in parts per million using the solvent as an internal standard ($CDCl_3$ at 7.28 ppm). NMR data are reported as s = singlet, d = doublet, t = triplet, q = quartet, p = pentet, m = multiplet, br = broad, app = apparent, and dd = doublet of doublets, and coupling constants are in hertz, followed by integration information. UV−vis−NIR spectra were measured with a Cary 5000 instrument. HRMS spectra were obtained with a QTOF HRMS instrument utilizing nanospray ionization. The mass analyzer was set to the 400−2000 Da range. Photostabiltiy studies were performed with a Xe lamp (SF-150-C, 150 W, AM 1.5 filter, ScienceTech solar simulator) and a cutoff filter blocking light of <400 nm from ThorLabs. Solution-phase fluorescent quantum yields were obtained using the optically dilute method described by Crosby and Demas.[49] All sample concentrations were on the order of 10^{-5} M to reduce reabsorption. The 647 nm line of a Kr^+/Ar^+ ion laser was used as the excitation source, and zinc phthalocyanine (ϕ = 0.30 in 1% pyridine in toluene)[50] was used as a reference. Fluorescence lifetimes were obtained by excitation with the 485 nm line of a pulsed diode laser (fwhm < 100 ps) and detection with an avalanche photodiode. Infrared spectra were recorded with an Agilent Cary 660 ATR-FTIR spectrometer.

2-(5-Dodecylthiophene-2-yl)furan (5). To a degassed mixture of **4** (4.4 g, 13.24 mmol) and $Pd(PPh_3)_4$ (1.6 g, 1.4 mmol) were added the dry toluene (60 mL) and dry *N*,*N*-dimethylformamide (60 mL). The solution was stirred at room temperature for 30 min before 2-(tri-*n*-butylstannyl)furan (4.6 mL, 14.5 mmol) was added. The mixture was stirred at room temperature for another 30 min before being heated to reflux for 48 h. After being cooled to room temperature and diluted with dichloromethane, the product was extracted with deionized water. The organic layers were combined, dried over $MgSO_4$, and concentrated under reduced pressure. The product was purified by flash column chromatography (petroleum ether) and obtained as a light beige oil in 84% yield (3.5 g). ^{1}H NMR (300 MHz, $CDCl_3$): δ 7.37 (s, 1H), 7.05 (d, J = 3.6 Hz, 1H), 6.70 (d, J = 3.6 Hz, 1H), 6.46−6.37 (m, 2H), 2.80 (t, J = 7.6 Hz, 2H), 1.68 (m, 2H), 1.48−1.31 (m, 18H), 0.89 (t, J = 6.9 Hz, 3H). ^{13}C NMR (75 MHz, $CDCl_3$): δ 149.9, 145.3, 141.3, 131.3, 124.7, 122.4, 111.7, 104.3, 32.1, 31.8, 30.2, 29.8, 29.7, 29.5, 29.2, 22.9, 14.3. HRMS (ESI): m/z calcd for $C_{20}H_{30}OS$ $[M + Cs]^+$ 451.1072, found 451.1091.

Tributyl(5-(5-dodecylthiophene-2-yl)furan-2-yl)stannane (3). Under argon, *n*-butyllithium in hexane (2.5 M, 2.4 mL, 6.0 mmol) was added to a solution of **5** (1.3 g, 4.0 mmol) in dry THF (40 mL) at −10 °C, and the mixture was stirred at this temperature for 30 min. Tributyltin chloride (1.6 mL, 1.6 mmol) was added, and the reaction mixture was warmed to room temperature and stirred for an additional 12 h. The reaction was then quenched with brine (50 mL), and the product was extracted with ethyl acetate. The organic layers were combined, washed with water, dried over $MgSO_4$, and concentrated under reduced pressure. The crude product was used directly without further purification. ^{1}H NMR (500 MHz, $CDCl_3$): δ 7.05 (d, J = 3.5 Hz, 1H), 6.70 (d, J = 3.5 Hz, 1H), 6.58 (d, J = 3.0 Hz, 1H), 6.45 (d, J = 3.1 Hz, 1H), 2.82 (t, J = 7.5 Hz, 2H), 1.72−1.59 (m, 8H), 1.53−1.47 (m, 6H), 1.42−1.30 (m, 24 H), 1.14−1.10 (m, 9H), 0.84−0.82 (m, 3H). HRMS (ESI): m/z calcd for $C_{32}H_{56}OSSnCs$ $[M + Cs]^+$ 741.2128, found 741.2147.

5,7-Bis(5′-dodecyl-[2,2′-bithiophene]-5-yl)-2,3-diphenylthieno[3,4-*b*]pyrazine (TPzPh(TT)$_2$). To a flame-dried sealed tube were added **1** (25 mg, 0.056 mmol), tributyl(5′-dodecyl-[2,2′-bithiophene]-5-yl)stannane (71.3 mg, 0.112 mmol), dimethylformamide (0.3 mL, 0.2 M) degassed for 20 min, and $PdCl_2(PPh_3)_2$ (0.014 mg, 0.006 mmol). The whole reaction was heated under N_2 while being stirred at 50 °C for 48 h. The reaction mixture was poured into ether, extracted with water, and dried with anhydrous Na_2SO_4. The product was purified through recrystallization with hot hexanes to give a green crystalline solid (6.4 mg, 12.0%). ^{1}H NMR (300 MHz, $CDCl_3$): δ 7.59 (d, J = 7.7 Hz, 6H), 7.39−7.35 (m, 6H), 7.09 (d, J = 3.7 Hz, 2H) 7.06 (d, J = 3.6 Hz, 2H), 6.71 (d, J = 3.5 Hz, 2H), 2.79 (t, J = 7.4 Hz, 4H), 1.72−1.67 (m, 4H), 1.34−1.27 (m, 36H), 0.92−0.86 (m, 6H). HRMS (ESI): m/z calcd for $C_{58}H_{68}N_2S_5Cs$ $[M + Cs]^+$ 1085.3041, found 1085.3046. IR (neat, cm^{-1}): 2953.4, 2920.3, 2852.2, 1723.4, 1459.3, 1377.4, 1260.3, 1094.2, 1019.2. Mp: 130.0−132.4 °C.

5,7-Bis(5-(5-dodecylthiophene-2-yl)furan-2-yl)-2,3-diphenylthieno[3,4-*b*]pyrazine (TPzPh(FT)$_2$). To a flame-dried sealed tube were added **1** (25 mg, 0.056 mmol), tributyl(5-(5-dodecylthiophene-2-yl)furan-2-yl)stannane (69.5 mg, 0.112 mmol), dimethylformamide (0.3 mL, 0.2 M) degassed for 20 min, and $PdCl_2(PPh_3)_2$ (0.014 mg, 0.006 mmol). The reaction was heated under N_2 with a sealed tube while being stirred at 50 °C for 48 h. The reaction mixture was poured into ether, extracted with water, and dried with anhydrous Na_2SO_4. The product was purified through recrystallization with hot hexane to give a green crystalline solid (5.8 mg, 11.0%). ^{1}H NMR (500 MHz, acetone-d_6): δ 7.64 (d, J = 7.0 Hz, 4H), 7.53 (d, J = 5.0 Hz, 2H), 7.46−7.40 (m, 6H), 7.36 (d, J = 5.0 Hz, 2H), 6.91 (d, J = 3.6 Hz, 2H), 6.88 (d, J = 3.6 Hz, 2H), 2.93 (t, J = 8.9 Hz, 4H), 1.79−1.74 (m, 4H), 1.47−1.32 (m, 36H), 0.90−0.88 (m, 6H). MS (ESI): m/z calcd for $C_{58}H_{68}N_2O_2S_3Cs$ $[M + Cs]^+$ 1053.3497, found 1053.3505. IR (neat, cm^{-1}): 2951.5, 2924.1, 2854.2, 1092.9, 1018.7. Mp: 126.0−129.4 °C.

5,5‴′-Didodecyl-3″,4″-dinitro-2,2′:5′,2″:5″,2‴:5‴,2‴′-quinquethiophene (7; X = TT). To a flame-dried round-bottom flask were added **6** (50 mg, 0.15 mmol), **2** (303 mg, 0.36 mmol), toluene (4.5 mL, 0.03 M), and $Pd(PPh_3)_4$ (4.5 mg, 0.004 mmol) under N_2. The reaction was sealed and heated with stirring for 24 h at 100 °C. The reaction mixture was extracted with DCM and water. The product was filtered through a pad of silica gel, and recrystallized with hexane to give a red solid (46 mg, 37%). ^{1}H NMR (500 MHz, $CDCl_3$): δ 7.47 (d, J = 7.0 Hz, 2H), 7.14 (app t, J = 3.9 Hz, 4H), 6.75 (d, J = 3.6 Hz, 2H), 2.83 (t, J = 7.6 Hz, 4H), 1.73−1.70 (m, 4H), 1.45−1.23 (m, 36H), 0.92−0.90 (m, 6H). ^{13}C NMR (125 MHz, $CDCl_3$): δ 147.9, 144.2, 135.2, 133.4, 132.9, 132.1, 125.7, 125.3, 125.2, 123.7, 31.9, 31.5, 30.3, 29.8, 29.7, 29.6, 29.5, 29.4, 29.3, 29.1, 22.7, 14.1. HRMS (ESI): m/z calcd for $C_{44}H_{58}N_2O_4S_5Cs$ $[M + Cs]^+$ 971.2054, found 971.2083. IR (neat, cm^{-1}): 2920.7, 2852.2, 1535.4, 1464.0. Mp: 111.6−114.1 °C.

5,5‴′-Didodecyl-[2,2′:5′,2″:5″,2‴:5‴,2‴′-quinquethiophene]-3″,4″-diamine (8; X = TT). To a N_2-filled round-bottom flask were added **7** (X = TT; 46 mg, 0.055 mmol), ethanol (0.34 mL, 0.16 M), DCM (0.34 mL, 0.16 M), and a solution of tin(II) chloride dihydrate (124 mg, 0.55 mmol) in ethanol (0.55 mL, 1.0 M) and concentrated HCl (0.41 mL, 1.35 M). The reaction was stirred for 3 days at 30 °C. The reaction mixture was quenched by 25% NaOH (aq) and extracted with DCM. The crude product was used immediately without further purification. ^{1}H NMR (300 MHz, $CDCl_3$): δ 7.07 (d, J = 3.7 Hz, 2H), 6.98 (app d, J = 3.5 Hz, 4H), 6.70 (d, J = 3.4 Hz, 2H). 2.81 (t, J = 7.3 Hz, 4H), 1.94−1.86 (m, 4H), 1.78−1.68 (m, 4H), 1.67−1.52 (m, 36H), 1.19−1.03 (m, 6H).

4,6-Bis(5′-dodecyl-[2,2′-bithiophene]-5-yl)thieno[3,4-*c*]-[1,2,5]thiadiazole (TTD(TT)$_2$). To a flame-dried round-bottom flask

DOI: 10.1021/acs.joc.7b00422
J. Org. Chem. 2017, 82, 5597−5606

were added **8** (X = TT; 17.5 mg, 0.022 mmol), pyridine (0.12 mL, 0.18 M), (TMS)Cl (0.012 mL, 0.154 mmol), and thionylaniline (0.003 mL, 0.044 mmol) sequentially under N_2. The reaction was stirred at room temperature overnight. The reaction was quenched with 1.0 M HCl (aq) and extracted with DCM. The product was purified through recrystallization with hot hexane to give a bright green solid (8.0 mg, 45%). ^{1}H NMR (500 MHz, $CDCl_3$): δ 7.47 (d, J = 3.6 Hz, 2H), 7.12 (d, J = 3.9 Hz, 2H), 7.08 (d, J = 3.3 Hz 2H), 6.73 (d, J = 3.4 Hz, 2H). 2.83 (t, J = 7.5 Hz, 4H), 1.74−1.68 (m, 4H), 1.44−1.31 (m, 36H), 0.92−0.89 (t, J = 6.5 Hz, 6H). HRMS (ESI): m/z calcd for $C_{44}H_{58}N_2S_6$ $[M]^+$ 806.2924, found 806.2903. IR (neat, cm^{-1}): 2953.3, 2917.3, 2849.6, 1462.3, 1258.5, 1020.5. Mp: 117.8−123.9 °C.

4,4′-(3,4-Dinitrothiophene-2,5-diyl)bis(*N*,*N*-bis(4-(hexyloxy)-phenyl)aniline) (7; X = TPA). To a flame-dried round-bottom flask were added **6** (40.0 mg, 0.12 mmol), TPA-Bpin (172.0 mg, 0.30 mmol), dioxane (20.0 mL, 0.006 M), K_2CO_3 (4.0 mL, 1.0 M), and $Pd(PPh_3)_4$ (70.7 mg, 0.061 mmol) under N_2. The reaction was heated to 90 °C and stirred overnight. The reaction was extracted with DCM and H_2O. The organic layer was then dried with sodium sulfate. The product was purified through column chromatography with 40% DCM/hexane to give a red solid (76.0 mg, 60%). ^{1}H NMR (500 MHz, $CDCl_3$): δ 7.62 (d, J = 8.2 Hz, 4H), 7.07 (d, J = 8.2 Hz, 8H), 6.88 (d, J = 8.0 Hz, 4H), 6.83 (d, J = 8.9 Hz, 4H), 3.95 (t, J = 6.5 Hz, 8H), 1.83−1.78 (m, 8H), 1.52−1.46 (m, 8H), 1.38−1.35 (m, 16H), 0.93 (t, J = 6.8 Hz, 12H). ^{13}C NMR (125 MHz, $CDCl_3$): δ 155.8, 151.5, 140.2, 135.8, 127.1, 119.2, 118.6, 115.4, 115.3, 83.4, 68.2, 31.6, 25.8, 24.9 22.7, 14.1. HRMS (ESI): m/z calcd for $C_{64}H_{75}N_4SO_8Cs$ $[M + Cs]^+$ 1193.4438, found 1193.4442. IR (neat, cm^{-1}): 2928.7, 2861.4, 1718.4, 1600.9, 1503.3, 1240.5. Mp: 124.1−128.2 °C.

2,5-Bis(4-(bis(4-(hexyloxy)phenyl)amino)phenyl)thiophene-3,4-diamine (8; X = TPA). **7** (X = TPA; 10 mg, 0.01 mmol) was dissolved in ethanol (0.06 mL, 0.16 M) and DCM (0.06 mL, 0.16 M) in a round-bottom flask under N_2. Tin(II) chloride dihydrate (22.6 mg, 0.1 mmol) was added as a solution in ethanol (0.1 mL, 1.0 M) and concentrated HCl (0.074 mL, 1.35 M) to the reaction mixture. The reaction was stirred for 3 days at 30 °C. The reaction was quenched with 25% NaOH (aq) and extracted with DCM to give a yellow oil. The crude product was directly used immediately in the next reaction without further purification. ^{1}H NMR (300 MHz, DMSO-d_6): δ 7.32 (d, J = 8.6 Hz, 4H), 6.99 (d, J = 8.7 Hz, 8H), 6.88 (d, J = 8.9 Hz, 8H), 6.79 (d, J = 8.7 Hz, 4H), 4.63 (s, 4H), 3.92 (t, J = 6.5 Hz, 8H), 1.72−1.67 (m, 8H), 1.41−1.23 (m, 24H), 0.88 (m, 12H).

4,4′-(Thieno[3,4-*c*][1,2,5]thiadiazole-4,6-diyl)bis(*N*,*N*-bis(4-(hexyloxy)phenyl)aniline) (TTD(TPA)$_2$). To a flame-dried round-bottom flask were added **8** (X = TPA; 43 mg, 0.04 mmol), *N*-thionylaniline (0.01 mL, 0.086 mmol), (TMS)Cl (0.04 mL, 0.301 mmol), and pyridine (0.24 mL, 0.18 M) under N_2. The reaction was stirred at room temperature overnight. The reaction was quenched with 1 M HCl (aq) and extracted with DCM to give a green solid. The product was purified through silica gel column chromatography with 40% DCM/hexane (17 mg, 39%). ^{1}H NMR (500 MHz, DMSO-d_6): δ 7.89 (d, J = 8.7 Hz, 4H), 7.06 (d, J = 8.9 Hz, 8H), 6.93 (d, J = 8.9 Hz, 8H), 6.86 (d, J = 8.7 Hz, 4H), 3.95 (t, J = 6.5 Hz, 8H), 1.73−1.70 (m, 8H), 1.46−1.39 (m, 8H), 1.34−1.21 (m, 24H), 0.91−0.86 (m, 12H). HRMS (ESI): m/z calcd for $C_{64}H_{76}N_4O_4S_2$ $[M + Cs]^+$ 1161.4363, found 1161.4347. IR (neat, cm^{-1}): 2924.9, 2856.7, 1600.8, 1505.3, 1480.5, 1240.1, 1030.6.

■ ASSOCIATED CONTENT

Supporting Information

The Supporting Information is available free of charge on the ACS Publications website at DOI: 10.1021/acs.joc.7b00422.

Absorption and emission spectra in variable solvents, ^{1}H and ^{13}C NMR spectra, HPLC data, and DFT Cartesian coordinates (PDF)

■ AUTHOR INFORMATION

Corresponding Author

*E-mail: delcamp@olemiss.edu. Web site: www.delcampgroup.com.

ORCID

Yanbing Zhang: 0000-0002-8622-0594
Shane A. Autry: 0000-0002-6872-7885
Louis E. McNamara: 0000-0002-7706-6441
Suong T. Nguyen: 0000-0002-5745-9096
Phillip Brogdon: 0000-0002-9625-8414
Davita L. Watkins: 0000-0002-0943-7220
Nathan I. Hammer: 0000-0002-6221-2709
Jared H. Delcamp: 0000-0001-5313-4078

Notes

The authors declare no competing financial interest.

■ ACKNOWLEDGMENTS

Y.Z., S.A.A., L.E.M., P.B., N.I.H., and J.H.D. thank the National Science Foundation for generous support through a Track 2 EPSCoR Award (OIA-1539035). D.L.W. appreciates financial support of this work from Oak Ridge Associated Universities through the Ralph E. Powe Award.

■ REFERENCES

(1) Keereweer, S.; Van Driel, P. B. A. A.; Snoeks, T. J. A.; Kerrebijn, J. D. F.; Baatenburg de Jong, R. J.; Vahrmeijer, A. L.; Sterenborg, H. J. C. M.; Löwik, C. W. G. M. *Clin. Cancer Res.* **2013**, *19*, 3745−3754.

(2) Bogaards, A.; Sterenborg, H. J. C. M.; Trachtenberg, J.; Wilson, B. C.; Lilge, L. *Lasers Surg. Med.* **2007**, *39*, 605−613.

(3) Mycek, M.-A.; Pogue, B. W. *Handbook of Biomedical Fluorescence*; CRC Press: New York, 2003; p 688.

(4) Smith, A. M.; Mancini, M. C.; Nie, S. *Nat. Nanotechnol.* **2009**, *4*, 710−711.

(5) Guo, Z.; Park, S.; Yoon, J.; Shin, I. *Chem. Soc. Rev.* **2014**, *43*, 16−29.

(6) Yi, X.; Wang, F.; Qin, W.; Yang, X.; Yuan, J. *Int. J. Nanomed.* **2014**, *9*, 1347−1365.

(7) For medicinal applications of ICG in surgery, see: (a) Alander, J. T.; Kaartinen, I.; Laakso, A.; Patila, T.; Spillmann, T.; Tuchin, V. V.; Venermo, M.; Välisuo, P. *Int. J. Biomed. Imaging* **2012**, *2012*, 940585. For cell imaging applications, see: (b) Yan, F.; Wu, H.; Liu, H.; Deng, Z.; Liu, H.; Duan, W.; Liu, X.; Zheng, H. *J. Controlled Release* **2016**, *224*, 217−228. For additional references on ICG, see: (c) Lee, H.; Mason, J. C.; Achilefu, S. *J. Org. Chem.* **2006**, *71*, 7862−7865. (d) Hirata, T.; Kogiso, H.; Morimoto, K.; Miyamoto, S.; Taue, H.; Sano, S.; Muguruma, N.; Ito, S.; Nagao, Y. *Bioorg. Med. Chem.* **1998**, *6*, 2179−2184. (e) Heseltine, D. W.; Brooker, L. G. S. U.S. Patent 2895955, 1959. (f) Gathje, J.; Steuer, R. R.; Nicholes, K. R. *J. Appl. Physiol.* **1970**, *29*, 181−185.

(8) Han, J.; Engler, A.; Qi, J.; Tung, C. H. *Tetrahedron Lett.* **2013**, *54*, 502−505.

(9) Davydenko, I.; Barlow, S.; Sharma, R.; Benis, S.; Simon, J.; Allen, T. G.; Cooper, M. W.; Khrustalev, V.; Jucov, E. V.; Castaneda, R.; Ordonez, C.; Li, Z.; Chi, S. H.; Jang, S. H.; Parker, T. C.; Timofeeva, T. V.; Perry, J. W.; Jen, A. K.; Hagan, D. J.; Van Stryland, E. W.; Marder, S. R. *J. Am. Chem. Soc.* **2016**, *138*, 10112−10115.

(10) Kim, J. S.; Kodagahally, R.; Strekowski, L.; Patonay, G. *Talanta* **2005**, *67*, 947−954.

(11) Nani, R. R.; Shaum, J. B.; Gorka, A. P.; Schnermann, M. J. *Org. Lett.* **2015**, *17*, 302−305.

(12) Peng, X.; Song, F.; Lu, E.; Wang, Y.; Zhou, W.; Fan, J.; Gao, Y. *J. Am. Chem. Soc.* **2005**, *127*, 4170−4171.

(13) Luo, S.; Zhang, E.; Su, Y.; Cheng, T.; Shi, C. *Biomaterials* **2011**, *32*, 7127−7138.

(14) Li, X.; Gao, X.; Shi, W.; Ma, H. *Chem. Rev.* **2014**, *114*, 590−659.

DOI: 10.1021/acs.joc.7b00422
J. Org. Chem. 2017, 82, 5597−5606

(15) Kaur, M.; Choi, D. H. *Chem. Soc. Rev.* **2015**, *44*, 58−77.
(16) Berezin, M. Y.; Achilefu, S. *Chem. Rev.* **2010**, *110*, 2641−2684.
(17) Sun, Y.; Qu, C.; Chen, H.; He, M.; Tang, C.; Shou, K.; Hong, S.; Yang, M.; Jiang, Y.; Ding, B.; Xiao, Y.; Xing, L.; Hong, X.; Cheng, Z. *Chem. Sci.* **2016**, *7*, 6203−6207.
(18) Zhang, X. D.; Wang, H.; Antaris, A. L.; Li, L.; Diao, S.; Ma, R.; Nguyen, A.; Hong, G.; Ma, Z.; Wang, J.; Zhu, S.; Castellano, J. M.; Wyss-Coray, T.; Liang, Y.; Luo, J.; Dai, H. *Adv. Mater.* **2016**, *28*, 6872−6879.
(19) Zhang, X.; Yu, H.; Xiao, Y. *J. Org. Chem.* **2012**, *77*, 669−673.
(20) Yamazawa, S.; Nakashima, M.; Suda, Y.; Nishiyabu, R.; Kubo, Y. *J. Org. Chem.* **2016**, *81*, 1310−1315.
(21) Ren, L.; Liu, F.; Shen, X.; Zhang, C.; Yi, Y.; Zhu, X. *J. Am. Chem. Soc.* **2015**, *137*, 11294−11302.
(22) Umezawa, K.; Citterio, D.; Suzuki, K. *Anal. Sci.* **2008**, *24*, 213−217.
(23) Avirah, R. R.; Jayaram, D. T.; Adarsh, N.; Ramaiah, D. *Org. Biomol. Chem.* **2012**, *10*, 911−920.
(24) Antaris, A. L.; Chen, H.; Cheng, K.; Sun, Y.; Hong, G.; Qu, C.; Diao, S.; Deng, Z.; Hu, X.; Zhang, B.; Zhang, X.; Yaghi, O. K.; Alamparambil, Z. R.; Hong, X.; Cheng, Z.; Dai, H. *Nat. Mater.* **2016**, *15*, 235−242.
(25) McNamara, L. E.; Liyanage, N.; Peddapuram, A.; Murphy, J. S.; Delcamp, J. H.; Hammer, N. I. *J. Org. Chem.* **2016**, *81*, 32−42.
(26) Tam, T. L.; Li, H.; Lam, Y. M.; Mhaisalkar, S. G.; Grimsdale, A. C. *Org. Lett.* **2011**, *13*, 4612−4615.
(27) Schwiderski, R. L.; Rasmussen, S. C. *J. Org. Chem.* **2013**, *78*, 5453−5462.
(28) Céron-Carrasco, J. P.; Siard, A.; Jacquemin, D. *Dyes Pigm.* **2013**, *99*, 972−978.
(29) Xia, Y.; Luo, J.; Deng, X.; Li, X.; Li, D.; Zhu, X.; Yang, W.; Cao, Y. *Macromol. Chem. Phys.* **2006**, *207*, 511−520.
(30) Kitamura, C.; Tanaka, S.; Yamashita, Y. *Chem. Mater.* **1996**, *8*, 570−578.
(31) Steinberger, S.; Mishra, A.; Reinold, E.; Mena-Osteritz, E.; Müller, H.; Uhrich, C.; Pfeiffer, M.; Bäuerle, P. *J. Mater. Chem.* **2012**, *22*, 2701−2712.
(32) Hwang, Y.-J.; Kim, F. S.; Xin, H.; Jenekhe, S. A. *Macromolecules* **2012**, *45*, 3732−3739.
(33) Mikroyannidis, J. A.; Tsagkournos, D. V.; Sharma, S. S.; Vijay, Y. K.; Sharma, G. D. *J. Mater. Chem.* **2011**, *21*, 4679−4688.
(34) Kmínek, I.; Výprachtický, D.; Kříž, J.; Dybal, J.; Cimrová, V. *J. Polym. Sci., Part A: Polym. Chem.* **2010**, *48*, 2743−2756.
(35) Bower, J. D.; Schlessinger, R. H. *J. Am. Chem. Soc.* **1969**, *91*, 6891−6892.
(36) Abdo, N. I.; El-Shehawy, A. A.; El-Barbary, A. A.; Lee, J.-S. *Eur. J. Org. Chem.* **2012**, *2012*, 5540−5551.
(37) Luo, J.; Zhao, B.; On Chan, H. S.; Chi, C. *J. Mater. Chem.* **2010**, *20*, 1932−1941.
(38) Lambert, C.; Scherpf, T.; Ceymann, H.; Schmiedel, A.; Holzapfel, M. *J. Am. Chem. Soc.* **2015**, *137*, 3547−3557.
(39) Siebrand, W. *J. Chem. Phys.* **1967**, *46*, 440−447.
(40) Siebrand, W. *J. Chem. Phys.* **1967**, *47*, 2411−2422.
(41) Caspar, J. V.; Sullivan, B. P.; Kober, E. M.; Meyer, T. J. *Chem. Phys. Lett.* **1982**, *91*, 91−95.
(42) Englman, R.; Jortner, J. *Mol. Phys.* **1970**, *18*, 145−164.
(43) Wilson, J. S.; Chawdhury, N.; Al-Mandhary, M. R. A.; Younus, M.; Khan, M. S.; Raithby, P. R.; Köhler, A.; Friend, R. H. *J. Am. Chem. Soc.* **2001**, *123*, 9412−9417.
(44) Cekli, S.; Winkel, R. W.; Alarousu, E.; Mohammed, O. F.; Schanze, K. S. *Chem. Sci.* **2016**, *7*, 3621−3631.
(45) Chen, X.; Peng, X.; Cui, A.; Wang, B.; Wang, L.; Zhang, R. *J. Photochem. Photobiol., A* **2006**, *181*, 79−85.
(46) Song, F.; Peng, X.; Lu, E.; Zhang, R.; Chen, X.; Song, B. *J. Photochem. Photobiol., A* **2004**, *168*, 53−57.
(47) Su, D.; Teoh, C. L.; Samanta, A.; Kang, N. Y.; Park, S. J.; Chang, Y. T. *Chem. Commun.* **2015**, *51*, 3989−3992.
(48) Kirkus, M.; Knippenberg, S.; Beljonne, D.; Cornil, J.; Janssen, R. A.; Meskers, S. C. *J. Phys. Chem. A* **2013**, *117*, 2782−2789.
(49) Crosby, G. A.; Demas, J. N. *J. Phys. Chem.* **1971**, *75*, 991−1024.
(50) Vincett, P. S.; Voigt, E. M.; Rieckhoff, K. E. *J. Chem. Phys.* **1971**, *55*, 4131−4140.

DOI: 10.1021/acs.joc.7b00422
J. Org. Chem. 2017, 82, 5597−5606